The GALAH survey: effective temperature calibration from the InfraRed Flux Method in the *Gaia* system

Luca Casagrande [1,2]★† Jane Lin,[1,2] Adam D. Rains [1] Fan Liu [3] Sven Buder [1,2]
Jonathan Horner [4] Martin Asplund,[5] Geraint F. Lewis [6] Sarah L. Martell [7,2]
Thomas Nordlander [1,2] Dennis Stello,[7,2] Yuan-Sen Ting,[1,2,8,9,10] Robert A. Wittenmyer,[4]
Joss Bland-Hawthorn [2,6] Andrew R. Casey [11,12] Gayandhi M. De Silva,[13,14] Valentina D'Orazi,[15]
Ken C. Freeman,[1] Michael R. Hayden,[2,6] Janez Kos,[16] Karin Lind,[17] Katharine J. Schlesinger,[1]
Sanjib Sharma [2,6] Jeffrey D. Simpson [2,7] Daniel B. Zucker[18,14] and Tomaž Zwitter [16]

[1]*Research School of Astronomy and Astrophysics, The Australian National University, Canberra, ACT 2611, Australia*
[2]*ARC Centre of Excellence for All Sky Astrophysics in 3 Dimensions (ASTRO 3D), Australia*
[3]*Centre for Astrophysics and Supercomputing, Swinburne University of Technology, Melbourne, VIC 3122, Australia*
[4]*Centre for Astrophysics, University of Southern Queensland, Toowoomba, QLD 4350, Australia*
[5]*Max Planck Institute for Astrophysics, Karl-Schwarzschild-Str 1, D-85748 Garching, Germany*
[6]*Sydney Institute for Astronomy, School of Physics, A28, The University of Sydney, NSW 2006, Australia*
[7]*School of Physics, UNSW, Sydney, NSW 2052, Australia*
[8]*Institute for Advanced Study, Princeton, NJ 08540, USA*
[9]*Department of Astrophysical Sciences, Princeton University, Princeton, NJ 08544, USA*
[10]*Observatories of the Carnegie Institution of Washington, 813 Santa Barbara Street, Pasadena, CA 91101, USA*
[11]*Monash Centre for Astrophysics, Monash University, 3800, Australia*
[12]*School of Physics and Astronomy, Monash University, 3800, Australia*
[13]*Australian Astronomical Optics, Faculty of Science and Engineering, Macquarie University, Macquarie Park, NSW 2113, Australia*
[14]*Macquarie University Research Centre for Astronomy, Astrophysics & Astrophotonics, Sydney, NSW 2109, Australia*
[15]*Istituto Nazionale di Astrofisica, Osservatorio Astronomico di Padova, vicolo dell'Osservatorio 5, I-35122 Padova, Italy*
[16]*Faculty of Mathematics and Physics, University of Ljubljana, Jadranska 19, 1000 Ljubljana, Slovenia*
[17]*Department of Astronomy, Stockholm University, AlbaNova University Centre, SE-106 91 Stockholm, Sweden*
[18]*Department of Physics and Astronomy, Macquarie University, Sydney, NSW 2109, Australia*

ABSTRACT

In order to accurately determine stellar properties, knowledge of the effective temperature of stars is vital. We implement *Gaia* and 2MASS photometry in the InfraRed Flux Method and apply it to over 360 000 stars across different evolutionary stages in the GALAH DR3 survey. We derive colour-effective temperature relations that take into account the effect of metallicity and surface gravity over the range $4000\,\mathrm{K} \lesssim T_{\mathrm{eff}} \lesssim 8000\,\mathrm{K}$, from very metal-poor stars to supersolar metallicities. The internal uncertainty of these calibrations is of order 40–80 K depending on the colour combination used. Comparison against solar-twins, *Gaia* benchmark stars, and the latest interferometric measurements validates the precision and accuracy of these calibrations from F to early M spectral types. We assess the impact of various sources of uncertainties, including the assumed extinction law, and provide guidelines to use our relations. Robust solar colours are also derived.

Key words: techniques: photometric – stars: abundances – stars: atmospheres – stars: fundamental parameters – stars: Hertzsprung–Russell and colour–magnitude diagrams – infrared: stars.

1 INTRODUCTION

The effective temperature (T_{eff}) is one of the most fundamental stellar parameters, and it affects virtually every stellar property that we determine, be it from spectroscopy, or inferred by comparing against stellar models (e.g. Choi et al. 2018; Nissen & Gustafsson 2018).

While angular diameters measured from interferometry provide the most direct way to measure effective temperatures of stars (provided bolometric fluxes can also be determined, see e.g. Code et al. 1976), they require a considerable investment of time. Such analysis require a careful assessment of systematic uncertainties, and they are biased towards bright targets, which are often saturated in modern photometric systems and all-sky surveys (e.g. White et al. 2013; Lachaume et al. 2019; Rains et al. 2020). Further, these stars are often the hardest to observe for large-scale spectroscopic surveys.

★ E-mail: luca.casagrande@anu.edu.au
† Colour-T_{eff} routines: https://github.com/casaluca/colte

Among the many indirect methods to determine $T_{\rm eff}$ is the InfraRed Flux Method (hereafter IRFM), an almost model-independent photometric technique originally devised to obtain angular diameters to a precision of a few per cent, and capable of competing against intensity interferometry in cases where a good flux calibration is achieved (Blackwell & Shallis 1977; Blackwell, Shallis & Selby 1979; Blackwell, Petford & Shallis 1980). Over the years, the IRFM has been successfully applied to determine the effective temperatures of stars of different spectral types and metallicities (e.g. Blackwell & Shallis 1977; Alonso, Arribas & Martinez-Roger 1996b, 1999; Ramírez & Meléndez 2005; González Hernández & Bonifacio 2009; Casagrande et al. 2010).

The version of the IRFM used in this work has been previously validated against solar twins, *HST* absolute spectrophotometry, and interferometric angular diameters (Casagrande, Portinari & Flynn 2006; Casagrande et al. 2010). In particular, dedicated near-infrared photometry has been carried out to derive effective temperatures of interferometric targets with saturated 2MASS magnitudes (Casagrande et al. 2014). Our $T_{\rm eff}$ scale is widely used by many studies and surveys, and we now make it available into the *Gaia* photometric system. To do so, we implement *Gaia* photometry into the IRFM described in Casagrande et al. (2006, 2010). Also, due to *Gaia* parallaxes it is now possible to derive reliable surface gravities. We provide colour−$T_{\rm eff}$ relations which take into account the effect of metallicity and surface gravity by running the IRFM for all stars in the third Data Release (DR3) of the GALAH survey (Buder et al. 2021). This data release also includes stars observed with the same instrument set-up, data reduction and analysis pipeline by the K2-HERMES (Wittenmyer et al. 2018; Sharma et al. 2019) and TESS-HERMES (Sharma et al. 2018) surveys.

We describe how *Gaia* photometry is implemented into our version of the IRFM in Section 2 and present colour−$T_{\rm eff}$ relations in Section 3. We benchmark our results against standard stars, assess the typical $T_{\rm eff}$ uncertainty of our calibrations, and provide guidelines for their use in Section 4. Finally, we comment on the use of different colour indices and draw our conclusions in Section 5.

2 THE INFRARED FLUX METHOD USING GAIA PHOTOMETRY

The IRFM can be viewed as the most extreme colour technique since it relies on the index defined by the ratio between the bolometric and the infrared monochromatic flux of a star. This ratio can be compared to that obtained using the same quantities defined on a stellar surface element, $\sigma T_{\rm eff}^4$ and $\mathcal{F}_{\rm IR}$(model), respectively (see e.g. Alonso, Arribas & Martinez-Roger 1996a; Casagrande et al. 2006). If stellar and model fluxes are known, it is then possible to solve for $T_{\rm eff}$. As we describe later, this step is done iteratively in our version of the IRFM. The crucial advantage of the IRFM over other colour techniques is that, at least for spectral types hotter than early M-type, near-infrared photometry samples the Rayleigh–Jeans tail of stellar spectra, a region largely dominated by the continuum,[1] with a roughly linear dependence on $T_{\rm eff}$. The model-dependent term $\mathcal{F}_{\rm IR}$(model) is almost unaffected by metallicity, surface gravity, and granulation, as extensively tested in the literature (e.g. Alonso et al. 1996b; Asplund & García Pérez 2001; Ramírez & Meléndez 2005; Casagrande et al. 2006; Casagrande 2009; González Hernández & Bonifacio 2009).

We use the implementation of the IRFM described in Casagrande et al. (2006, 2010), where for each star we now use *Gaia BP*, *RP*, and 2MASS *JHK$_s$* photometry to derive the bolometric flux. The flux outside these bands (i.e. the bolometric correction) is estimated using a theoretical model flux at a given $T_{\rm eff}$, log(g), and [Fe/H]. The infrared monochromatic flux is derived from 2MASS magnitudes only. An iterative procedure in $T_{\rm eff}$ is adopted to cope with the mildly model-dependent nature of the bolometric correction and surface infrared monochromatic flux. We interpolate over the Castelli & Kurucz (2003) grid of model fluxes, starting for each star with an initial estimate of its effective temperature and adopting the GALAH DR3 [Fe/H] and log(g), until convergence in $T_{\rm eff}$ is reached within 1 K. The convergence is robust regardless of the initial $T_{\rm eff}$ estimate. The model dependence is expected to be small, and in Casagrande et al. (2006, 2010) we tested that using the MARCS grid of model fluxes (Gustafsson et al. 2008) affects the resulting $T_{\rm eff}$ only by few K for dwarfs and subgiants in the range $\simeq$ 4500–6500 K.

For *Gaia BP* and *RP* magnitudes we use the `Gaia-DR2` formalism described in Casagrande & VandenBerg (2018), which is based on the revised transmission curves and non-revised Vega zero-points provided by Evans et al. (2018). As described in Casagrande & VandenBerg (2018), this choice best mimics the photometric processing done by the *Gaia* team to reproduce `phot_g_mean_mag`, `phot_bp_mean_mag`, and `phot_rp_mean_mag` given in *Gaia* DR2. In Appendix A, we also implement *Gaia* EDR3 photometry, and provide calibrations for this system. We remark that although *Gaia* EDR3 is formally an independent photometric systems from *Gaia* DR2, differences are overall small for the sake of the $T_{\rm eff}$ derived from the IRFM (although the calibrations in the two systems should not be used interchangeably, as further discussed in Appendix A). We use *BP* and *RP* instead of *G* magnitudes for a number of reasons: comparison with absolute spectrophotometry indicates that *BP* and *RP* are reliable and well standardized in the magnitude range $\simeq$ 5 to 16, which is relevant for our targets. On the contrary, *G* magnitudes have a magnitude-dependent offset, and are affected by uncalibrated CCD saturation for $G \lesssim 6$ (Casagrande & VandenBerg 2018; Evans et al. 2018; Maíz Apellániz & Weiler 2018). Further, the *BP* and *RP* bandpasses together have the same wavelength coverage as the *G* bandpass.

One of the most critical points when implementing the IRFM is the photometric absolute calibration (i.e. how magnitudes are converted into fluxes), which sets the zero-point of the $T_{\rm eff}$ scale. This is particularly important in the infrared, for which we use the same 2MASS prescriptions discussed in Casagrande et al. (2010). To verify that the zero-point of our $T_{\rm eff}$ scale is not altered by *Gaia* magnitudes, we derive $T_{\rm eff}$ for all stars in Casagrande et al. (2010) with a counterpart in *Gaia* (408 targets). Not unexpectedly, we find excellent agreement, with both mean and median $\Delta T_{\rm eff} = 12 \pm 2$ K ($\sigma = 41$ K) and no trends as a function of stellar parameters. This difference is robust, regardless of whether the stars used are those with the best *Gaia* quality flags. Although this difference is fully within the 20 K zero-point uncertainty of the reference $T_{\rm eff}$ scale of Casagrande et al. (2010), we correct for this small offset to adhere to the parent scale.

We apply the IRFM to over 620 000 spectra in GALAH DR3 for which [Fe/H], log(g), *BP*, *RP*, *J*, *H*, *K$_s$* are available. About 40 per cent of the targets have $E(B - V)$ from Green et al. (2019). For the remaining stars, we rescale reddening from Schlegel, Finkbeiner & Davis (1998) with the same procedure described in Casagrande et al. (2019). Effective temperatures from the IRFM along with adopted values of reddening are available as part of GALAH DR3 (Buder et al. 2021, which also includes a comparison against the GALAH

---

[1] See however Blackwell, Lynas-Gray & Petford 1991 for a discussion of the importance of H$^-$ opacity.
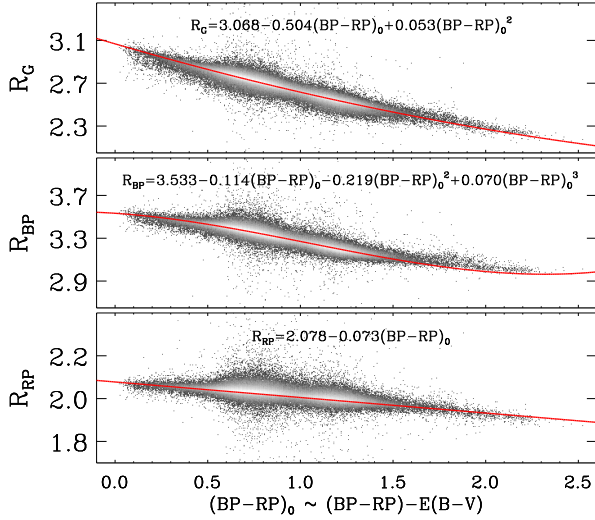
Figure 1. *Gaia* extinction coefficients as a function of intrinsic stellar colours for our sample of stars (colour-coded in grey by log-density). The red solid lines show the fits given in each panel. To estimate intrinsic colours needed for the fits, one can iterate starting from $(BP - RP)_0 \simeq (BP - RP) - E(B - V)$. See Appendix B for a summary of the extinction coefficients for *Gaia* DR2, EDR3, and 2MASS under different extinction laws.

Figure 2. Left-hand panel: colour–$T_{\rm eff}$ relation obtained from the IRFM in $(G - RP)_0$, where extinction coefficients are computed for each star individually. Right-hand panel: colour–$T_{\rm eff}$ relation using the same input effective temperatures, but constant extinction coefficients to deredden the colour index. The importance of using variable extinction coefficients becomes visible for increasing values of reddening. Stars are colour-coded by their $E(B - V)$ with the distribution shown in the inset.

spectroscopic $T_{\rm eff}$.). To account for the spectral type dependence of extinction coefficients, in the IRFM we adopt the Cardelli, Clayton & Mathis (1989)/O'Donnell (1994) extinction law, and for each star compute extinction coefficients with the synthetic spectrum at the $T_{\rm eff}$, $\log(g)$, and [Fe/H] used at each iteration.

Fig. 1 shows extinction coefficients for the *Gaia* filters as a function of intrinsic (i.e. reddening-corrected) stellar colour for our sample of stars. For the 2MASS system there is virtually no dependence on spectral type and the following constant values are found $R_J = 0.899$, $R_H = 0.567$, and $R_{Ks} = 0.366$. These coefficients are in excellent agreement with those reported in Casagrande & VandenBerg (2014, 2018), obtained using the same extinction law. We discuss in Appendix B the effect of using different extinction laws on the derived colour$-T_{\rm eff}$ relations and extinction coefficients.

The use of constant extinction coefficients instead of colour-dependent ones affects colour indices, and hence the effective temperatures derived from the relations of Section 3. This can be appreciated from the comparison in Fig. 2, where the difference in colour obtained using constant or colour-dependent extinction coefficients is amplified at high values of reddening for a given input $T_{\rm eff}$. The fits of Fig. 1 should thus be preferred to deredden colour indices involving *Gaia* bands, especially in regions of high extinction.

3 COLOUR$-T_{\rm EFF}$ RELATIONS

In order to derive colour–$T_{\rm eff}$ relations, we first apply a few quality cuts. We restrict ourselves to stars with the best GALAH DR3 spectroscopic parameters (flag_sp=0), and *Gaia* photometry $1.0 + 0.015 (BP - RP)^2 <$ phot_bp_rp_excess_factor $< 1.3 + 0.060 (BP - RP)^2$ and phot_proc_mode=0. There is a sharp drop in the number of stars with $G > 14$, and this reflects the GALAH selection function. Only 5 per cent of stars are fainter than 14, and 0.06 per cent are in the faintest bin $16 < G \lesssim 16.5$. For relations involving the G band we also exclude a handful of stars with $G < 6$ (Evans et al. 2018; Riello et al. 2018). These requirements yield automatically good 2MASS photometry: median photometric
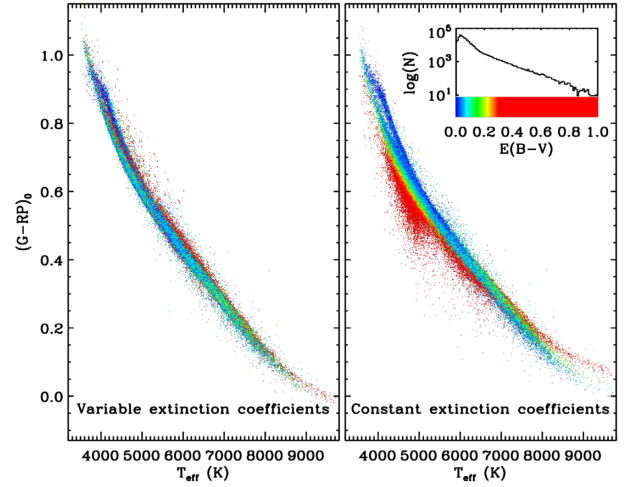
errors in JHK_s are 0.024 mag with 99.9 per cent of the targets having 2MASS quality flag Qflg='AAA'.

Depending on the combination of filters, there are over 360 000 stars available for our fits. We use only stars with $E(B - V) < 0.1$ to derive our fits, to avoid a strong dependence on the adopted extinction law (Appendix B). Due to the combined effect of the GALAH selection function and target selection effects (most notably stellar evolutionary time-scales), the distribution of targets has two main temperature overdensities: one at the main-sequence turn-off and the other at the red-clump phase. If all available stars were used to derive colour$-T_{\rm eff}$ relations these two overdensities would dominate the fit. Instead, we sample our stars uniformly in $T_{\rm eff}$, randomly selecting 20 stars every 20 K, and repeating this for 10 realizations. The calibration sample for each fit is thus based on roughly 50 000 stars. We repeat the above procedure 10 000 times, and select the fit that returns the lowest standard deviation with respect to the input effective temperatures from the IRFM. We also explored the effect of a uniform gridding in $T_{\rm eff}$ and $\log(g)$ but did not find any significant difference with respect to a uniform sampling in $T_{\rm eff}$ only.

To derive our relations we started with a polynomial as a function of colour, which is the parameter that has the strongest dependence on $T_{\rm eff}$. Depending on the colour index, we found that a third- or fifth-order polynomial was necessary to describe the curve inflection occurring at low $T_{\rm eff}$. We then added the [Fe/H] and $\log(g)$ dependence into the fit. The *Gaia* broad-band filters have a rather mild dependence on metallicity, and the effect of $\log(g)$ is most noticeable below 4500 K, where colour–$T_{\rm eff}$ relations for dwarf and giant stars branch off (Figs 3 and 4). We found no need to go higher than first order in [Fe/H] and $\log(g)$, but cross-terms with colour, as well as a term involving colour, $T_{\rm eff}$, and $\log(g)$ were found to improve the fit. The adopted functional form is

$$T_{\rm eff} = a_0 + a_1 X + a_2 X^2 + a_3 X^3 + a_4 X^5 + a_5 \log(g) + a_6 \log(g) X$$

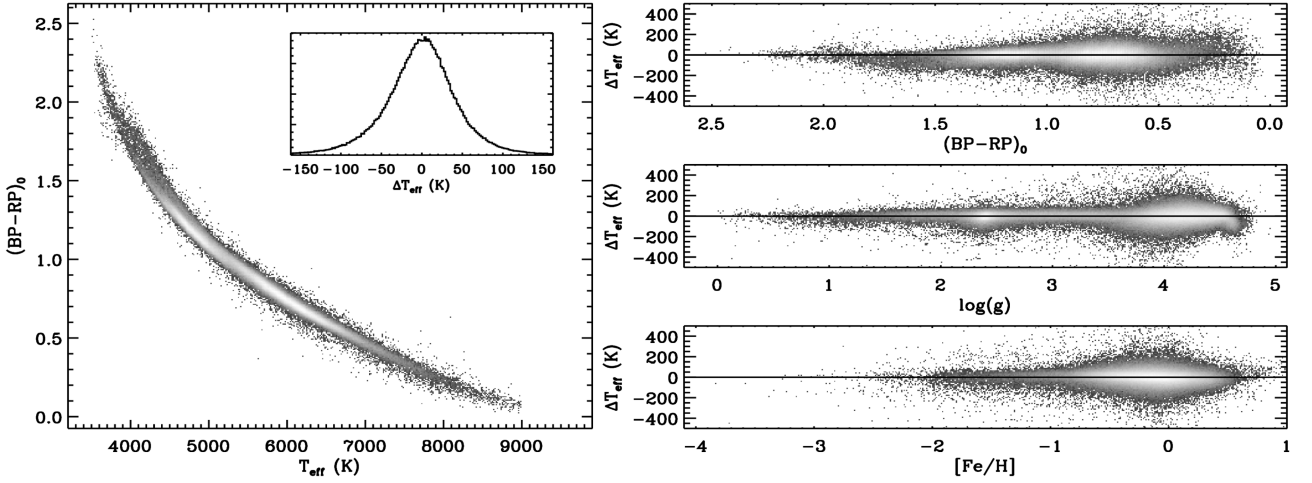$$+ a_7 \log(g) X^2 + a_8 \log(g) X^3 + a_9 \log(g) X^5 + a_{10} [{\rm Fe/H}]$$

Figure 3. Left-hand panel: log-density plot of the colour–T_{eff} relation obtained using all 360 000 GALAH DR3 stars with good photometric and spectroscopic flags as described in the text. For $T_{eff} \lesssim 4500$ K the two loci defined by dwarf and giant stars can be noticed. The inset shows the distribution of the T_{eff} residuals of our calibration. Right-hand panels: T_{eff} residuals plotted as a function of colour, surface gravity, and metallicity. Plots for the other colour indices are available as supplementary online material.
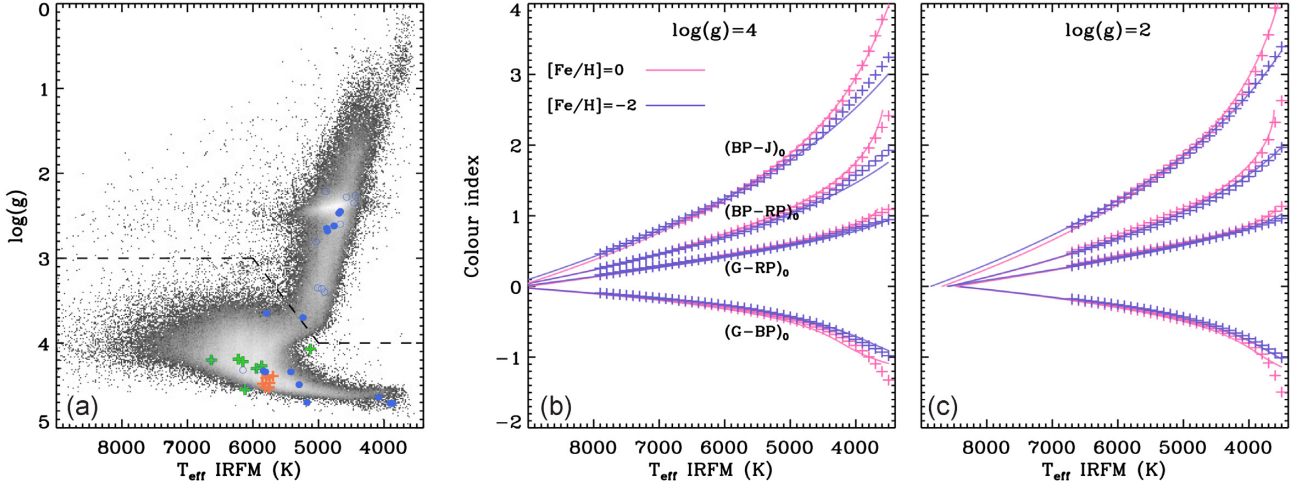

Figure 4. Panel (a): Kiel diagram of the GALAH DR3 sample used to derive the colour–T_{eff} relations presented in this work. The dashed line marks the separation between dwarf and giant stars discussed in Section 4. The coloured crosses and circles are the stars used in Fig. 6 to test the T_{eff} scale. Panels (b) and (c): some of the colour–T_{eff} relations (solid lines) of Table 1 for fixed values of $\log(g) = 4$ and $\log(g) = 2$, and [Fe/H] = 0 and [Fe/H] = −2, as labelled. Plotted for comparison are synthetic colour–T_{eff} computed for the same values of gravity and metallicity (cross symbols). Note that the maximum T_{eff} available for synthetic colours varies with the adopted $\log(g)$.

$$a_{11}[\text{Fe/H}]\,X + a_{12}[\text{Fe/H}]\,X^2 + a_{13}[\text{Fe/H}]\,X^3$$
$$+\, a_{14}[\text{Fe/H}]\log(g)\,X, \qquad (1)$$

where X is the colour index corrected for reddening, and not all terms were found to be significant for all colour indices. The coefficients of equation (1) are given in Table 1. Our relations and associated standard deviations are derived over the range $3600\,\text{K} \lesssim T_{eff} \lesssim 9000\,\text{K}$, although as we discuss in the next section, they are validated by independent measurements over a smaller range of effective temperatures. Polynomial fits are also typically less robust towards the edges of a colour index. In Table 2, we recommend conservative colour ranges, which effectively limit the applicability of our relations between 4000 and 8000 K for most filter combinations.

Fig. 3 shows the colour–T_{eff} relation for $(BP - RP)_0$, along with the residuals of the fit as a function of colour, gravity, and metallicity. Although equation (1) virtually allows for any combination of input parameters, it should be recalled that stars distribute across the HR diagram as permitted by stellar evolutionary theory. Fig. 4(a) illustrates the range of stars used to build our colour calibrations, where cool stars are found both at low and high surface gravities, while the hottest stars have $\log(g) \sim 4$. Figs 4(b) and (c) show the dependence on $\log(g)$ and [Fe/H] for some of our colour–T_{eff} calibrations. In addition, to allow direct comparison, we also plot predictions from synthetic stellar fluxes computed with the bolometric-corrections[2] code (Casagrande & VandenBerg 2014, 2018). The purpose of this comparison is not to validate

[2]https://github.com/casaluca/bolometric-corrections

Table 1. Coefficients of the $T_{\rm eff}$ calibration of equation (1) suitable for *Gaia* DR2 photometry. See Appendix A for *Gaia* EDR3 photometry.

colour	a_0	a_1	a_2	a_3	a_4	a_5	a_6	a_7	a_8	a_9	a_{10}	a_{11}	a_{12}	a_{13}	a_{14}	$\sigma(T_{\rm eff})$ (K)
$(BP - RP)_0$	7928	−3663.1140	803.3017	−9.3727	–	325.1324	−500.1160	279.4832	−53.5062	–	−2.4205	−128.0354	49.4933	5.9146	41.3650	54–66
$(G - BP)_0$	7555	5803.7715	–	−2441.7124	437.7314	455.0997	2243.1333	3669.4924	1872.7035	–	19.1085	75.2198	–	–	−83.9777	75–93
$(G - RP)_0$	7971	−5737.5049	–	1619.9946	−203.8234	255.7408	−492.8268	160.1957	103.1114	–	−64.3289	34.3339	–	–	54.7224	56–4
$(BP - J)_0$	8218	−2526.8430	458.1827	−28.4540	–	234.0113	−205.3084	63.4781	−7.2083	–	−85.7048	−50.1557	32.3428	−2.3553	20.0671	44–49
$(BP - H)_0$	8462	−2570.3684	537.5968	−44.3644	–	189.1198	−106.7584	31.1720	−4.9137	–	−9.2587	−189.8600	75.8619	−6.8592	16.7226	33–42
$(BP - K_s)_0$	8404	−2265.1355	403.4693	−27.9056	–	193.5820	−145.3724	47.7998	−6.4572	–	−34.5438	−130.2559	52.6470	−4.4777	15.8249	24–32
$(RP - J)_0$	9074	−7670.6606	3164.0525	–	−126.1476	–	−7.3816	−12.5168	–	−2.0452	–	76.1144	–	–	−45.8056	90–95
$(RP - H)_0$	8924	−4779.3394	1319.8989	–	−16.6676	–	−23.6583	22.4243	–	−4.3066	–	35.0102	–	–	−28.7228	52–62
$(RP - K_s)_0$	8940	−4450.6138	1138.6816	–	−10.5749	–	−42.3037	33.3365	–	−3.2535	–	41.0402	–	–	−21.9922	43–48
$(G - J)_0$	8370	−3559.7710	895.8869	−86.7011	–	180.7568	−164.9264	24.4263	4.2318	–	−127.9640	72.1449	–	–	13.7683	54–57
$(G - H)_0$	8186	−2536.7671	503.2762	−42.7871	–	230.4871	−254.5291	104.6258	−17.4859	–	−122.0732	45.0572	–	–	6.9992	37–41
$(G - K_s)_0$	8103	−1857.7194	–	73.1834	−1.7576	236.0335	−345.9070	170.4915	−28.8549	–	−131.4548	49.6232	–	–	10.0777	27–32

Note.. *G* magnitudes have been corrected following Maíz Apellániz & Weiler (2018): $G + 0.0271(6 - G)$ for $G \leq 6$, $G - 0.0032(G - 6)$ for $6 < G < 16$ and $G - 0.032$ for $G \geq 16$. These corrections should be applied before using our relations with *G* magnitudes: the effect on indices with short colour baseline such as $(G - BP)_0$ and $(G - RP)_0$ is noticeable, and up to 100–200 K for hot stars in particular. See Table B1 for extinction coefficients suitable for *Gaia* DR2 and 2MASS. Users should also be wary of applying colour–$T_{\rm eff}$ relations to stars with $G < 6$ and *BP* and *RP* brighter than ~5 due to the saturation of bright magnitudes in *Gaia*. For the standard deviation of the calibration $\sigma(T_{\rm eff})$, we provide two estimates, both obtained using all available ~ 360 000 stars, instead of the ~ 50 000 used to derive fits. The first one is the precision of the fits, whereas for the second one input [Fe/H] and log (*g*) are perturbed with a Gaussian random noise of 0.2 and 0.5 dex, respectively. Note that an extra uncertainty of about 20 K on the zero-point of our effective temperature scale should still be added.

Table 2. Recommended colour range for the validity of our calibrations.

colour	dwarfs	giants
$(BP - RP)_0$	[0.20, 2.00]	[0.20, 2.55]
$(G - BP)_0$	[−1.00, −0.15]	[−1.40, −0.15]
$(G - RP)_0$	[0.15, 0.85]	[0.15, 1.15]
$(BP - J)_0$	[0.25, 3.00]	[0.90, 4.20]
$(BP - H)_0$	[0.40, 4.00]	[0.40, 4.90]
$(BP - K_s)_0$	[0.30, 4.20]	[0.30, 5.30]
$(RP - J)_0$	[0.20, 1.05]	[0.60, 1.55]
$(RP - H)_0$	[0.20, 1.60]	[0.20, 2.45]
$(RP - K_s)_0$	[0.20, 1.85]	[0.20, 2.70]
$(G - J)_0$	[0.15, 2.10]	[1.00, 2.80]
$(G - H)_0$	[0.25, 2.60]	[0.25, 3.70]
$(G - K_s)_0$	[0.20, 2.80]	[0.20, 3.90]

Note.. Dwarfs and giants are separated as per Fig. 4(a).

empirical or theoretical relations, but to show that our functional form well captures the expected change of colours with $T_{\rm eff}$, log (*g*), and [Fe/H]. Some of the discrepancies between empirical and theoretical predictions at the coolest $T_{\rm eff}$ are likely due to inadequacies of synthetic fluxes as discussed in the literature (see e.g. Casagrande & VandenBerg 2014; Böcek Topcu et al. 2020).

4 VALIDATION AND UNCERTAINTIES

We validate our colour–$T_{\rm eff}$ relations using three different test populations and approaches, focusing on Solar twins, *Gaia* Benchmark Stars (GBS), and interferometric measurements. The stars used for this purpose are some of the brightest and best observed in the sky, with careful determinations of their stellar parameters. In all instances, we apply the same requirements on `phot_bp_rp_excess_factor` and `phot_proc_mode` discussed in Section 3 to select the best photometry. We also exclude stars with $G < 6$ and *BP* and *RP* < 5 due to uncalibrated systematics at bright magnitudes. We only use 2MASS photometry with `Qflg='A'` in a given band.

The sample of solar twins is the same that was used by Casagrande et al. (2010) to set the zero-point of their $T_{\rm eff}$ scale. These twins are all nearby, unaffected by reddening, and with good *Gaia* and 2MASS photometry. Accurate and precise spectroscopic $T_{\rm eff}$, log (*g*), and [Fe/H] are available from differential analysis of high-resolution, high S/N spectra with respect to a solar reference spectrum, using excitation and ionization balance of iron lines (Meléndez, Dodds-Eden & Robles 2006; Meléndez et al. 2009). In particular, the identification of the best twins is based on the measured relative difference in equivalent widths and equivalent widths versus excitation potential relations with respect to the observed solar reference spectrum, and thus entirely model independent. In Table 3, we report the mean difference between the effective temperatures we derive in a given colour index, and the spectroscopic ones. Our $T_{\rm eff}$ are typically within few degrees of the spectroscopic ones. Further, regardless of the spectroscopic effective temperatures, the mean and median $T_{\rm eff}$ for our sample of solar twins in any colour index is always within few tens of K of the solar $T_{\rm eff}$. The fact that our colour–$T_{\rm eff}$ relations are well calibrated around the solar value is not unexpected, but confirms that we have achieved our goal of tying the current $T_{\rm eff}$ scale to that of Casagrande et al. (2010). To further test our scale, we use a large sample of more than 80 solar twins from Nissen (2015) and Spina et al. (2018). Also these twins have highly accurate and precise stellar parameters due to differential spectroscopic analysis. This means that in the comparison we are essentially dominated by photometric errors and intrinsic uncertainty in our colour–$T_{\rm eff}$ relations. The comparison

Table 3. Mean difference and standard deviation between the effective temperatures derived from our calibrations, and those from the literature used for validation (ours−literature). N is the number of stars available in each colour index.

Colour	Solar twins		GBS		Interferometry[†]	
	$\langle\Delta T_{eff}\rangle$	N	$\langle\Delta T_{eff}\rangle$	N	$\langle\Delta T_{eff}\rangle$	N
$(BP-RP)_0$	-3 ± 17	8	3 ± 34	7	-8 ± 49	15
$(G-BP)_0$	-30 ± 16	8	-19 ± 42	5	-10 ± 68	7
$(G-RP)_0$	0 ± 22	8	10 ± 31	5	-12 ± 55	7
$(BP-J)_0$	-6 ± 23	8	10 ± 55	5	9 ± 48	3
$(BP-H)_0$	10 ± 13	8	49 ± 48	5	95 ± 8	2
$(BP-K_s)_0$	-14 ± 21	8	-16 ± 32	6	-30 ± 60	6
$(RP-J)_0$	-13 ± 69	8	2 ± 108	5	-42 ± 112	3
$(RP-H)_0$	-2 ± 36	8	25 ± 74	5	68 ± 14	2
$(RP-K_s)_0$	-28 ± 37	8	-52 ± 40	6	-51 ± 59	6
$(G-J)_0$	-2 ± 36	8	-4 ± 72	5	-16 ± 49	3
$(G-H)_0$	5 ± 20	8	18 ± 59	5	60 ± 50	2
$(G-K_s)_0$	-27 ± 26	8	-52 ± 40	5	-54 ± 74	5

Note. [†]Only interferometric T_{eff} better than 1 per cent are used.

in Fig. 5 shows that the standard deviations for each colour index are consistent with the values reported in Table 1, although the latter are derived over a much larger range of stellar parameters. For solar-type stars $(BP-RP)_0$, $(G-BP)_0$, and $(G-RP)_0$ are the colours with the highest precision, while the use of RP photometry with 2MASS is the least informative, as it carries a typical uncertainty of order 100 K. The standard error of the mean shows that individual colours can have systematic offsets of a few tens of K at most: although calibrations are built on to a set of input values, small local deviations are inherent to polynomial functional forms (see e.g. Ramírez & Meléndez 2005). When deriving T_{eff} from colour relations, users should be mindful of the trade-off between choosing the colour index(es) with the highest

precision versus using as many indices as possible to average down systematic errors (often at the cost of precision). If one were to use the mean T_{eff} from all indices, the mean difference with respect to the spectroscopic measurements in Fig. 5 would be 4 ± 5 K with a standard deviation $\sigma = 48$ K.

For the GBS we use T_{eff}, $\log(g)$, and [Fe/H] from the latest version of the catalogue (Jofré et al. 2018). The number of stars with good photometry varies depending on the filter used, with many of the GBS often having unreliable or saturated *Gaia* and/or 2MASS magnitudes. All GBS in our sample are closer than $\simeq 130$ pc, justifying the adoption of zero reddening. Again, we find overall excellent agreement between the T_{eff} we predict from colours, and those given in the GBS catalogue.

Finally, we assemble a list of interferometric measurements from the recent literature: Bigot et al. (2011), Boyajian et al. (2012a,b), Huber et al. (2012), Maestro et al. (2013), White et al. (2013, 2018), Gallenne et al. (2018), Baines et al. (2018), Rains et al. (2020), and Karovicova et al. (2020). For all these stars, we adopt reddening, $\log(g)$, and [Fe/H] reported in the above papers. This list encompasses over 200 targets, although most of them are very bright, hence with unreliable *Gaia* and/or 2MASS magnitudes, reducing the sample usable for our comparison to at most 33 targets, depending on the colour index. For M dwarfs we only retain stars with $(BP-RP)_0 \leq 2$ since this is roughly the reddest colour of dwarfs in GALAH DR3. Note that giant stars go to redder colours (up to 2.5, cf. Fig. 3), although interferometric T_{eff} of giants are available only for warmer temperatures. For the comparison in Table 3 we further require interferometric T_{eff} to be better than 1 per cent, which is the target accuracy at which we aim in testing. Allowing for larger uncertainties results in an increase of scatter in the comparison, with a trend whereby interferometric T_{eff} are systematically cooler for those stars with the largest uncertainties. This is indicative that systematic errors tend to overresolve angular diameters, hence underpredict
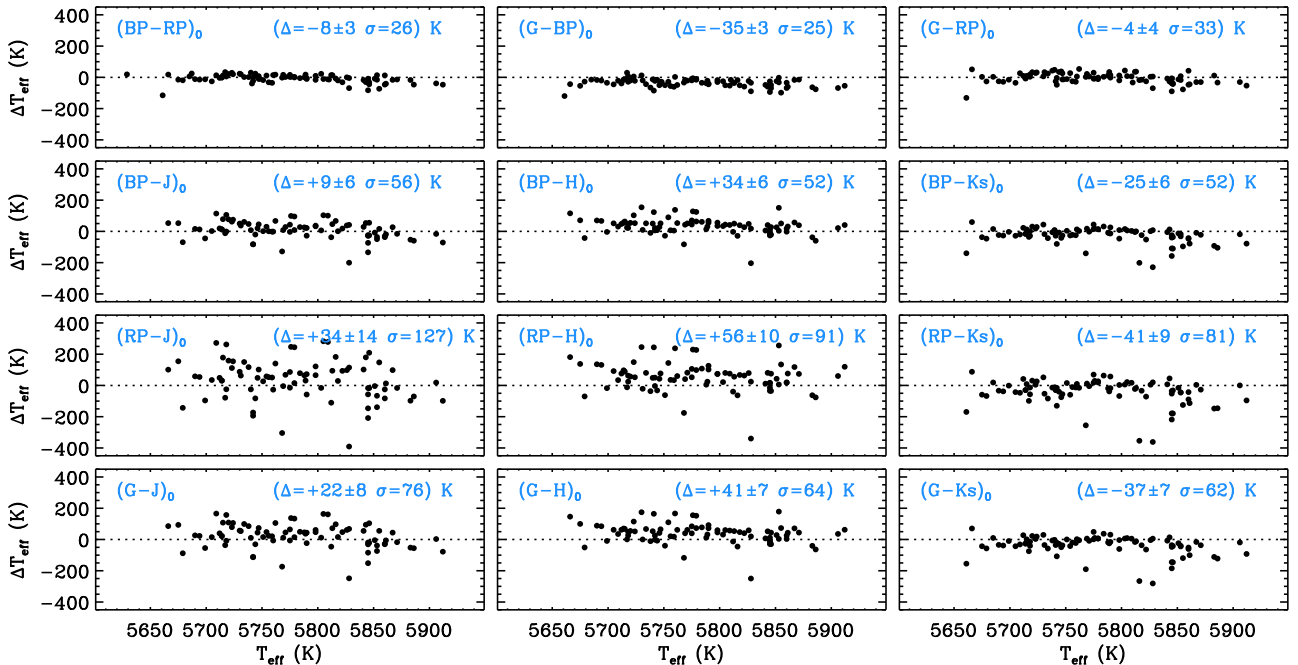

Figure 5. Comparison between the effective temperatures obtained from our calibrations and those derived by Nissen (2015) and Spina et al. (2018) from differential spectroscopic analysis of solar twins (x-axes). All targets are closer than 100 pc and unaffected by reddening. In each panel we report the colour index used, the mean difference Δ(ours − spectroscopy) ± standard error of the mean, and standard deviation (σ). Median and mean differences agree to within a few K.
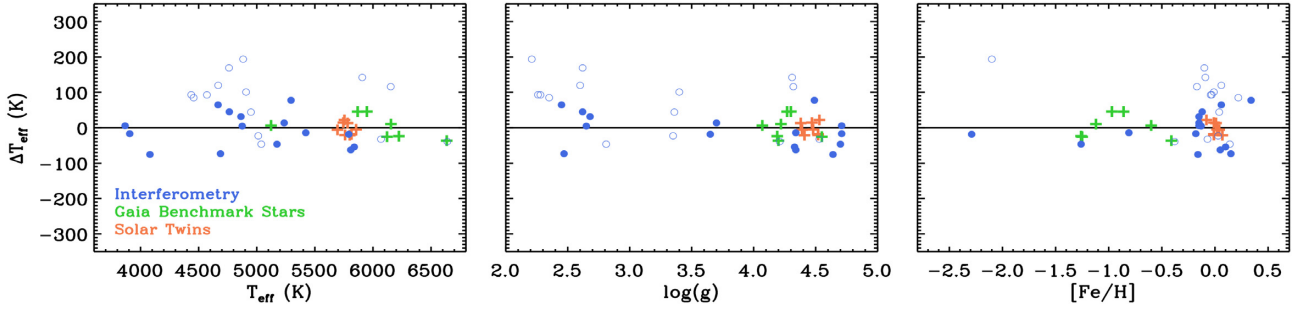
Figure 6. Comparison between T_{eff} derived using our $(BP - RP)_0$ relation and those available (ours−literature) for solar twins (orange), *Gaia* Benchmark Stars (blue), and interferometry (green). The filled and open circles indicate interferometric T_{eff} better than 1 and 2 per cent, respectively.
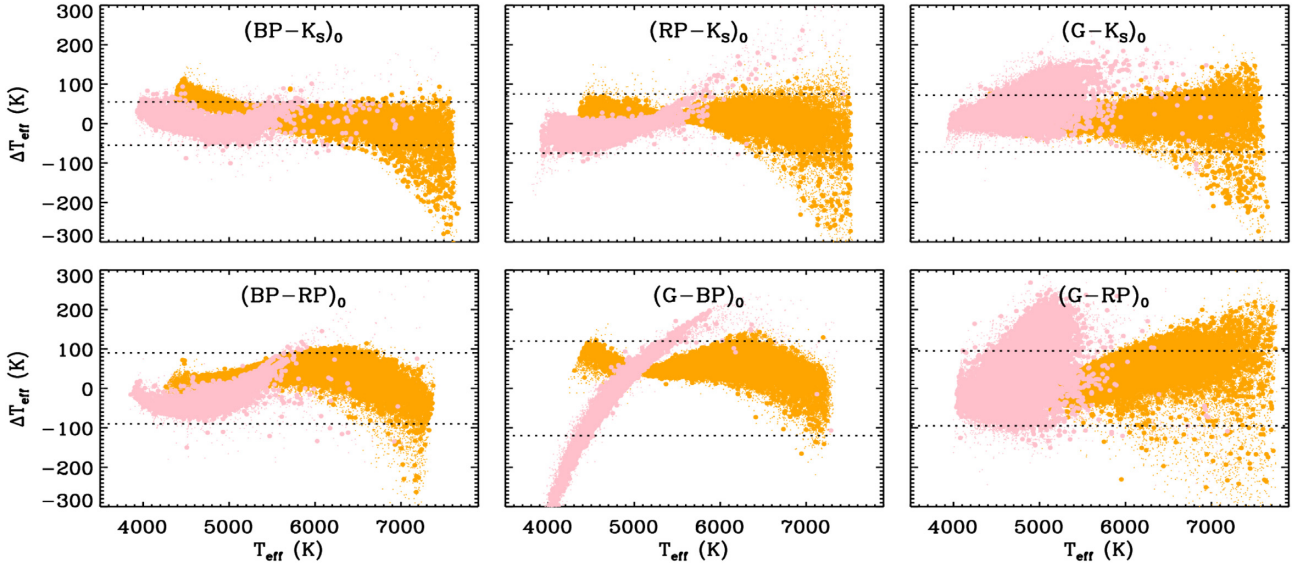

Figure 7. Comparison between T_{eff} derived using our relations and those of Mucciarelli & Bellazzini (2020, MB20) in the sense (ours−MB20). The relations of MB20 do not account for $\log(g)$, but are provided separately for dwarf (orange) and giant (pink) stars. Here, we use the separation (dwarfs versus giants) defined by the dashed line of Fig. 4 and apply the relations within their colour range. The same input [Fe/H] and dereddened photometry are used for both us and MB20. The filled circles are stars for which T_{eff} from our relations are within 10 K of the IRFM, to ensure differences are not stemming from the functional form of our polynomials. The dotted lines are the squared root of the squared sum of the typical uncertainty quoted for each colour–T_{eff} relation.

effective temperatures (see discussion in Casagrande et al. 2014). Also, interferometric targets with the largest T_{eff} uncertainties are often affected by relatively high values of reddening, which adds to the error budget.

Overall, it is clear from Table 3 that our relations are able to predict T_{eff} values in very good agreement with those reported in the literature for various benchmark samples. Depending on the colour index, mean differences are typically of order few tens of K. Occasional larger differences are still within the scatter of the relations, or are likely the result of small number statistics. When we restrict our analysis to the $(BP - RP)_0$ colour index, which has the largest number of stars available for comparison, the mean agreement is always within a few K regardless of the sample used (Fig. 6).

Finally, we compare our relations against those of Mucciarelli & Bellazzini (2020), which are the only ones also available for dwarf and giant stars in the *Gaia* DR2 system. The colour–T_{eff} relations of Mucciarelli & Bellazzini (2020) are built using several hundred stars with T_{eff} derived from the IRFM work of González Hernández & Bonifacio (2009). For dwarf stars, the T_{eff} scale of González Hernández & Bonifacio (2009) agrees well with that of Casagrande et al. (2010, which underpins our study), with a nearly

constant offset of 30–40 K (our scale being hotter) due to the different photometric absolute calibrations adopted. The same offset is thus expected for Mucciarelli & Bellazzini (2020). This is explored in Fig. 7, which shows the difference between the effective temperatures obtained using our relations against those of Mucciarelli & Bellazzini (2020) for colour indices in common. The first thing to notice is that the difference is not a constant offset, but varies as a function of T_{eff}, evolutionary status (dwarfs or giants), and colour index. To ensure this trend does not stem from the functional form of our polynomials, we have highlighted with filled circles stars for which our colour relations reproduce input T_{eff} from our IRFM to within 10 K. If one were to take the mean offset, it would typically be around few tens of K, with a maximum of order 50 K for $(G - RP)_0$ and $(G - BP)_0$, our scale being hotter. Overall, for most stars and colour indices, T_{eff} from our relations agree with those from Mucciarelli & Bellazzini (2020) to within ∼100 K, which is the uncertainty expected when combining the precision (standard deviation) reported for both calibrations. Indices with short colour baseline such as $(G - RP)_0$ or $(G - BP)_0$ display stronger systematic trends, in particular giants in $(G - BP)_0$. Larger deviations are also seen around and above 7000 K for dwarf stars, likely due to the

paucity of hot stars available to Mucciarelli & Bellazzini (2020) to constrain well their calibration at high temperatures. Part of the trends might also arise from the fact than many of the calibrating giants in Mucciarelli & Bellazzini (2020) have $G < 6$, a regime where *Gaia* DR2 photometry is affected by uncalibrated systematics. For our relations, we have also corrected the standardization of *Gaia* DR2 G magnitudes following Maíz Apellániz & Weiler (2018). Mucciarelli, Bellazzini & Massari (2021) provide updated relations using *Gaia* EDR3 photometry. As discussed in Appendix A, there are only minor differences between Figs 7 and A3 for $(BP - RP)_0$, $(BP - K_s)_0$, and $(RP - K_s)_0$. This is not surprising, given the overall agreement of the colour–T_{eff} relations for *Gaia* DR2 and EDR3. However, indices involving G magnitudes display reduced trends, which in part might arise from the better standardization of G-band photometry in EDR3.

From a user point of view, it is important to have realistic estimates of the precision at which T_{eff} can be estimated from our relations. In Table 1, we report two values for the standard deviation of our colour–T_{eff} relations. The first value is the precision of the fits. The second value provides a more realistic assessment of the uncertainties encountered when applying our relations, and is obtained by randomly perturbing the input [Fe/H] and $\log(g)$ with a Gaussian distribution of width 0.2 and 0.5 dex, respectively. The effect of a systematic shift of the GALAH $\log(g)$ and [Fe/H] scale by ± 0.2 and ± 0.1 dex, respectively, is typically also of a few tens of K at most. It should be kept in mind that uncertainties in the input stellar parameters will propagate differently with different colours, the effect being strongest for the coolest stars. Users of our calibrations are encouraged to assess their uncertainties on a case-by-case basis, by propagating the errors in their input parameters through equation (1). Further, an extra uncertainty of 20 K should still be added to account for the zero-point uncertainty of our T_{eff} scale (from Casagrande et al. 2010, see discussion in Section 2). We provide the code colte^3 to derive T_{eff} from our colour relations, taking into account the applicability ranges of Table 2, and with the option to derive realistic uncertainties through a MonteCarlo for each colour index. Other notable options include the choice of different extinction laws, and *Gaia* DR2 or EDR3 photometry.

Although our calibrations take into account the effect of surface gravity, there might be instances where the input $\log(g)$ is not known, besides a rough 'dwarf' versus 'giant' classification. To assess this impact, we classify stars as dwarfs (giants) if their gravities are higher (lower) than the dashed line of Fig. 4(a). We then adopt a constant $\log(g) = 4$ for dwarfs and $\log(g) = 2$ for giants. The effect of such an assumption on the derived T_{eff} is typically small, as can be seen in Fig. 8. The largest differences occur for stars in the upper giant branch, where assuming a constant $\log(g) = 2$ becomes inappropriate for $\log(g) \lesssim 1$–1.5. This effect can be quite strong for certain colour indices. In this case, one might use the fact that there is a strong correlation between the intrinsic colour and the surface gravity of stars along the RGB for a better assignment of $\log(g)$.

5 CONCLUSIONS

In this paper, we have implemented the *Gaia* DR2 and EDR3 photometric system in the IRFM and applied to over 360 000 stars with good spectroscopic and photometric flags to derive T_{eff} for stars across different evolutionary phases. In the literature, colour–T_{eff} relations for late type-stars are typically given separately for dwarfs and giants. The advent of *Gaia* parallaxes allows us to use robust
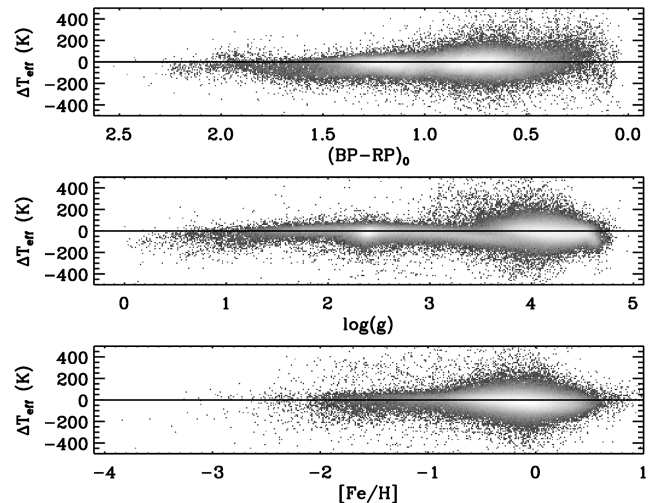
Figure 8. T_{eff} residual for the $(BP - RP)_0$ calibration when stars are assigned a fixed $\log(g) = 2$ or 4 based on their classification as giants or dwarfs as per Fig. 4. Plots for the other colour indices are available as supplementary online material.

surface gravities together with [Fe/H] from the GALAH DR3 survey to provide colour–T_{eff} relations that take into account the effect of these two parameters. Our calibrations are built and tested using the largest high-resolution stellar spectroscopic survey to date and cover a wide range of stellar colours and parameters: $0 \lesssim \log(g) \lesssim 4.8$ and $-3 \lesssim$ [Fe/H] $\lesssim 0.6$. When using our relations, users should refer to Figs 3 and 4 to have a sense for the parameter space covered, and for the performances of different colour indices. Users should always be mindful of the trade-off between choosing the colour index(es) with the highest precision versus using as many indices as possible to average down systematic errors, often at the cost of precision. $(BP - K_s)_0$ and $(G - K_s)_0$ are the indices which are best calibrated against T_{eff} across the parameter space, whereas indices leveraging on RP are the least performing ones. In particular, $(RP - J)_0$ has a very short colour baseline and the largest scatter, and other colour indices should be used instead, if possible. Moving to indices built only with *Gaia* filters, $(BP - RP)_0$ is the best choice, although $(G - BP)_0$ and $(G - RP)_0$ are also informative. For solar twins, all three indices return T_{eff} with remarkably small scatter with respect to the highly precise ones derived from differential spectroscopic analyses. Robust solar colours have also been derived (Appendix C). For most colour indices, our calibrations have a typical 1σ uncertainty of 40–80 K for the colour intervals of Table 2, which cover the region between 4000 and 8000 K. For 4000 K $\lesssim T_{eff} \lesssim 6700$ K our calibrations are also validated against solar twins, *Gaia* Benchmark Stars and interferometry.

ACKNOWLEDGEMENTS

DATA AVAILABILITY

The data underlying this article were accessed from the GALAH survey DR3 which can be queried using TAP at https://datacentral.org.au/vo/tap. The derived data generated in this research will be shared on reasonable request to the corresponding author.

REFERENCES

Alonso A., Arribas S., Martinez-Roger C., 1996a, A&AS, 117, 227
Alonso A., Arribas S., Martinez-Roger C., 1996b, A&A, 313, 873
Alonso A., Arribas S., Martínez-Roger C., 1999, A&AS, 140, 261
Asplund M., García Pérez A. E., 2001, A&A, 372, 601
Baines E. K., Armstrong J. T., Schmitt H. R., Zavala R. T., Benson J. A., Hutter D. J., Tycner C., van Belle G. T., 2018, AJ, 155, 30
Bigot L. et al., 2011, A&A, 534, L3
Blackwell D. E., Shallis M. J., 1977, MNRAS, 180, 177
Blackwell D. E., Shallis M. J., Selby M. J., 1979, MNRAS, 188, 847
Blackwell D. E., Petford A. D., Shallis M. J., 1980, A&A, 82, 249
Blackwell D. E., Lynas-Gray A. E., Petford A. D., 1991, A&A, 245, 567
Böcek Topcu G. et al., 2020, MNRAS, 491, 544
Boyajian T. S. et al., 2012a, ApJ, 746, 101
Boyajian T. S. et al., 2012b, ApJ, 757, 112
Buder S. et al., 2021, MNRAS, 506, 150
Cardelli J. A., Clayton G. C., Mathis J. S., 1989, ApJ, 345, 245
Casagrande L., 2009, Mem. Soc. Astron. Italiana, 80, 727
Casagrande L., VandenBerg D. A., 2014, MNRAS, 444, 392
Casagrande L., VandenBerg D. A., 2018, MNRAS, 479, L102
Casagrande L., Portinari L., Flynn C., 2006, MNRAS, 373, 13
Casagrande L., Ramírez I., Meléndez J., Bessell M., Asplund M., 2010, A&A, 512, A54
Casagrande L., Ramírez I., Meléndez J., Asplund M., 2012, ApJ, 761, 16
Casagrande L. et al., 2014, MNRAS, 439, 2060
Casagrande L., Wolf C., Mackey A. D., Nordland er T., Yong D., Bessell M., 2019, MNRAS, 482, 2770
Castelli F., Kurucz R. L., 2003, in Piskunov N., Weiss W. W., Gray D. F., eds, Proc. IAU Symp. 210, Modelling of Stellar Atmospheres. Kluwer, Dordrecht, p. A20
Choi J., Dotter A., Conroy C., Ting Y. S., 2018, ApJ, 860, 131
Code A. D., Bless R. C., Davis J., Brown R. H., 1976, ApJ, 203, 417
Evans D. W. et al., 2018, A&A, 616, A4
Fitzpatrick E. L., 1999, PASP, 111, 63
Gaia Collaboration, 2021, A&A, 649, A8
Gallenne A. et al., 2018, A&A, 616, A68
González Hernández J. I., Bonifacio P., 2009, A&A, 497, 497
Green G. M., Schlafly E., Zucker C., Speagle J. S., Finkbeiner D., 2019, ApJ, 887, 93
Gustafsson B., Edvardsson B., Eriksson K., Jørgensen U. G., Nordlund Å., Plez B., 2008, A&A, 486, 951
Huber D. et al., 2012, ApJ, 760, 32
Jofré P., Heiter U., Tucci Maia M., Soubiran C., Worley C. C., Hawkins K., Blanco-Cuaresma S., Rodrigo C., 2018, Res. Notes Am. Astron. Soc., 2, 152
Karovicova I., White T. R., Nordlander T., Casagrand e L., Ireland M., Huber D., Jofré P., 2020, A&A, 640, A25
Lachaume R., Rabus M., Jordán A., Brahm R., Boyajian T., von Braun K., Berger J. P., 2019, MNRAS, 484, 2656
Maestro V. et al., 2013, MNRAS, 434, 1321
Maíz Apellániz J., Weiler M., 2018, A&A, 619, A180
Meftah M. et al., 2018, A&A, 611, A1
Meléndez J., Dodds-Eden K., Robles J. A., 2006, ApJ, 641, L133
Meléndez J., Asplund M., Gustafsson B., Yong D., 2009, ApJ, 704, L66
Mucciarelli A., Bellazzini M., 2020, Res. Notes Am. Astron. Soc., 4, 52
Mucciarelli A., Bellazzini M., Massari D., 2021, preprint (arXiv:2106.03882)
Nissen P. E., 2015, A&A, 579, A52
Nissen P. E., Gustafsson B., 2018, A&AR, 26, 6
O'Donnell J. E., 1994, ApJ, 422, 158
Prša A. et al., 2016, AJ, 152, 41
Rains A. D., Ireland M. J., White T. R., Casagrande L., Karovicova I., 2020, MNRAS, 493, 2377
Ramírez I., Meléndez J., 2005, ApJ, 626, 465
Rieke G. H. et al., 2008, AJ, 135, 2245
Riello M. et al., 2018, A&A, 616, A3
Riello M. et al., 2021, A&A, 649, A3
Schlafly E. F., Finkbeiner D. P., 2011, ApJ, 737, 103
Schlegel D. J., Finkbeiner D. P., Davis M., 1998, ApJ, 500, 525
Sharma S. et al., 2018, MNRAS, 473, 2004
Sharma S. et al., 2019, MNRAS, 490, 5335
Spina L. et al., 2018, MNRAS, 474, 2580
Thuillier G., Floyd L., Woods T. N., Cebula R., Hilsenrath E., Hersé M., Labs D., 2004, Adv. Space Res., 34, 256
White T. R. et al., 2013, MNRAS, 433, 1262
White T. R. et al., 2018, MNRAS, 477, 4403
Wittenmyer R. A. et al., 2018, AJ, 155, 84

SUPPORTING INFORMATION

Supplementary data are available at *MNRAS* online.

Figure 3. Left-hand panel: log-density plot of the colour–T_{eff} relation obtained using all 360 000 GALAH DR3 stars with good photometric and spectroscopic flags as described in the text.

Figure 8. T_{eff} residual for the $(BP - RP)_0$ calibration when stars are assigned a fixed $\log(g) = 2$ or 4 based on their classification as giants or dwarfs as per Fig. 4.

Please note: Oxford University Press is not responsible for the content or functionality of any supporting materials supplied by the authors. Any queries (other than missing material) should be directed to the corresponding author for the article.

APPENDIX A: COLOUR–T_{EFF} RELATIONS USING GAIA EDR3 PHOTOMETRY

The IRFM and colour–T_{eff} relations described in the paper are based on *Gaia* DR2 photometry. Here, we discuss the implementation of *Gaia* EDR3 photometry into the IRFM and provide colour–T_{eff} relations for this system.

Gaia EDR3 photometry defines an independent photometric system from *Gaia* DR2, with significant improvements in the processing of the data and photometric calibration (see Riello et al. 2021, for an in-depth discussion). These improvements affect not only the published EDR3 magnitudes (and fluxes), but also the filter transmission curves and zero-points defining the system. Here, we implement EDR3 passbands and zero-points, along with EDR3 *BP* and *RP* photometry into the IRFM. As described in Section 2, 2MASS *JHK$_s$* are used in the infrared. Also in this instance we do not use the redundant information from EDR3 *G* magnitudes in the IRFM, although we do provide calibrations involving this band. *BP*, *RP*, and *G* magnitudes for bright sources have been corrected for saturation
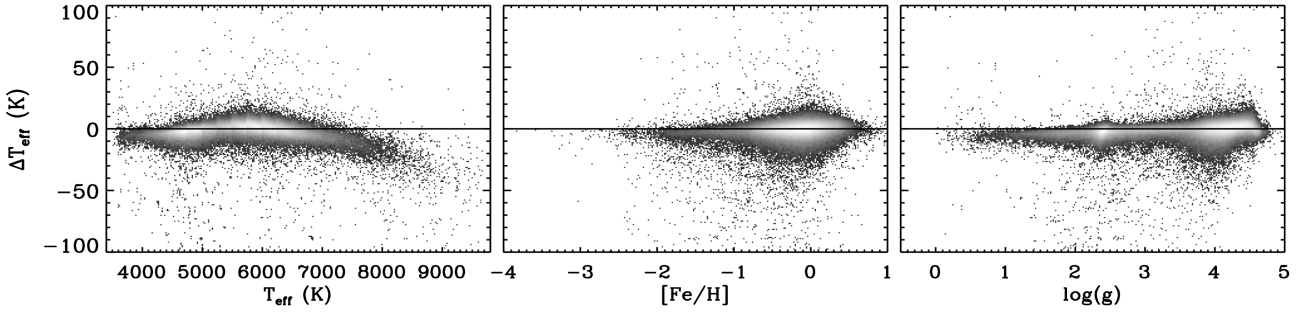
Figure A1. Log-density plot of the difference in effective temperatures derived by the IRFM when implementing *Gaia* EDR3 photometry instead of DR2 in the optical (EDR3 minus DR2). Approximately 355 000 stars with good GALAH spectroscopic, and photometric flags in both EDR3 and DR2 are shown here. For 96 per cent of the stars the difference is always within ±10 K.
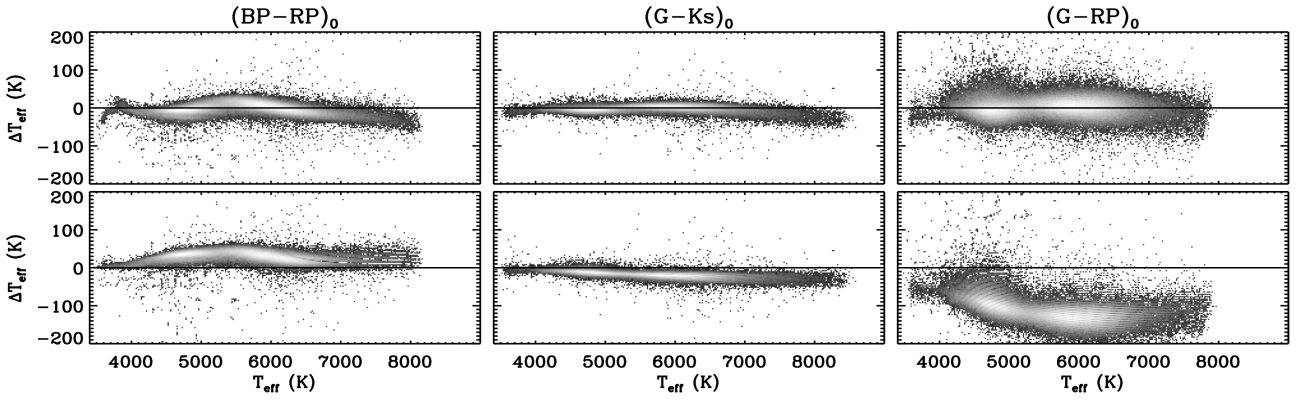
Figure A2. Top panels: log-density plots of the effective temperature difference between the *Gaia* EDR3 and DR2 calibration when photometry from the corresponding release is used. Bottom panels: effective temperature difference between using both EDR3 and DR2 photometry into the EDR3 calibration. The offset in $(G - RP)_0$ largely originates from the correction applied to DR2 G magnitudes (see discussion in the text). In all instances, calibrations have been applied within the validity ranges of Table 2.

Figure A3. Same as Fig. 7, but comparing our *Gaia* EDR3 relations against those of Mucciarelli et al. (2021).

effects following Riello et al. (2021). G magnitude correction for bright blue sources is not applied since none of our target is bluer than $BP - RP \sim 0$, but we correct G magnitudes for sources with two- or six-parameter astrometric solutions.[4]

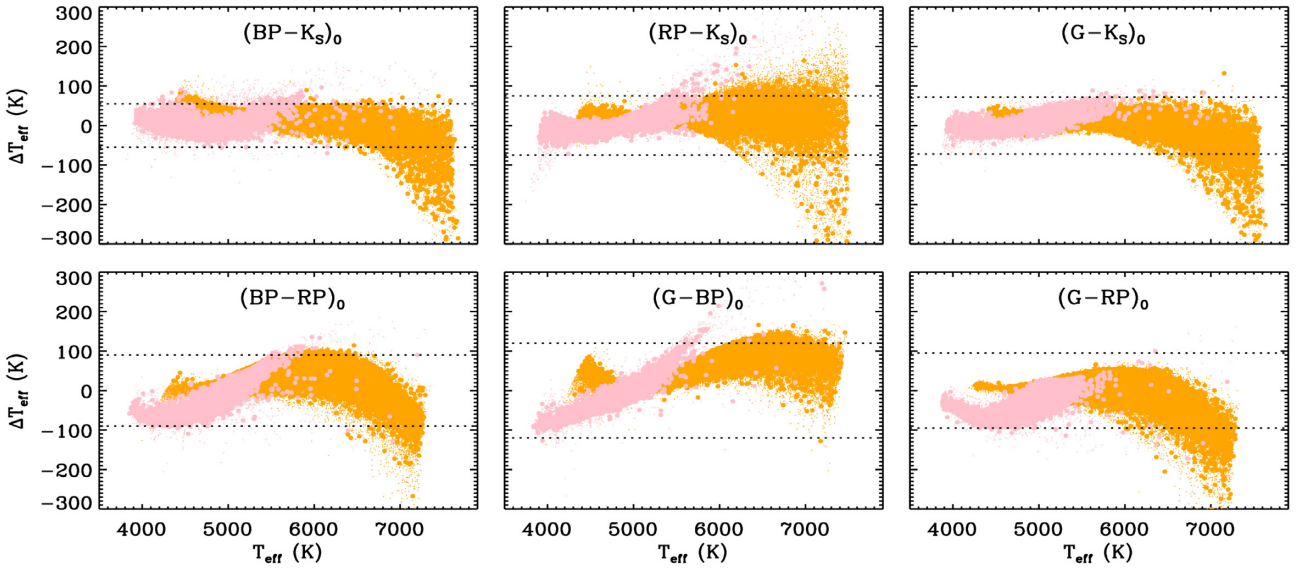As in Section 2, we derive T_{eff} for all stars in Casagrande et al. (2010) with a counterpart in EDR3 (now 410 targets), obtaining a mean and median $\Delta T_{eff} = 17 \pm 2$ K ($\sigma = 41$ K). The mean T_{eff} difference of implementing *Gaia* EDR3 instead of DR2 photometry is a mere 5 K with a slight trend as a function of T_{eff}. The latter is more clearly visible when comparing effective temperatures obtained from the IRFM for the entire GALAH sample (Fig. A1). For 96 (99) per cent of stars the difference is always within ± 10 K (± 20 K), well within the zero-point uncertainty of our scale, and no noticeable trends with surface gravity and metallicity. Above 7500 K however there is the tendency for EDR3 to return effective temperatures which are systematically cooler by some tens of K.

Table A1 provides colour–T_{eff} coefficients derived in a similar fashion to Table 1, but using instead EDR3 photometry. We select good photometry by requesting `phot_proc_mode=0` and BP and RP corrected excess factor[5] $-0.08 < C^\star < 0.2$ (Riello et al. 2021). This last requirement is similar to $0.001 + 0.039(BP - RP) < \log_{10}(phot\_bp\_rp\_excess\_factor) < 0.12 + 0.039(BP - RP)$ used by Gaia Collaboration (2021) to select good photometry. Note that extinction coefficients for *Gaia* EDR3 filters are also updated from Fig. 1, and provided in Table B1.

It is important to note that although the calibration for *Gaia* DR2 and EDR3 are overall similar, photometry from one system should never be used with the calibration of the other. The danger of doing this is shown for a few selected colour combinations in Fig. A2. On the top panels, when photometry from a data release is used with its colour–T_{eff} relation, the agreement between effective temperatures is consistent with that expected from Fig. A1 (as calibrations in different indices have their own intrinsic scatter). However, if – say – photometry from DR2 is used on to the calibration for EDR3 (equivalent of plotting the difference of the relations at same colour), systematic offsets will appear. This is particularly relevant for indices involving G magnitudes, which for *Gaia* DR2 have been corrected following Maíz Apellániz & Weiler (2018). Although this correction is magnitude dependent, over the range of our stars it amounts to few hundredths of a magnitude. This difference does not significantly impact T_{eff} in colours with long baseline, see e.g. $(G - K_s)_0$ in the bottom mid-panel of Fig. A2. However, for indices such as $(G - BP)_0$ or $(G - RP)_0$, effective temperatures can be off by as much as 100–200 K (bottom right panel of Fig. A2).

Although G magnitudes for sources with two- or six-parameter astrometric solutions still need minor corrections in EDR3, zero-point shifts to improve standardization are not necessary anymore (cf. Casagrande & VandenBerg 2018; Maíz Apellániz & Weiler 2018, for *Gaia* DR2). Similarly, many of the bright objects used by Mucciarelli et al. (2021) to define their relations have much improved G-band photometry in EDR3. This likely explains the reduced trends when comparing our EDR3 calibrations against those of Mucciarelli et al. (2021) for indices involving G band (see Fig. A3 and discussion in Section 4).

[4] https://github.com/agabrown/gaiaedr3-6p-gband-correction
[5] https://github.com/agabrown/gaiaedr3-flux-excess-correction

Table A1. Coefficients of the T_{eff} calibration of equation (1) suitable for *Gaia* EDR3 photometry.

Colour	a_0	a_1	a_2	a_3	a_4	a_5	a_6	a_7	a_8	a_9	a_{10}	a_{11}	a_{12}	a_{13}	a_{14}	$\sigma(T_{eff})$ (K)
$(BP - RP)_0$	7981	−4138.3457	1264.9366	−130.4388	–	285.8393	−324.2196	106.8511	−4.9825	–	4.5138	−203.7774	126.6981	−14.7442	40.7376	55–64
$(G - BP)_0$	7346	5810.6636	−2880.3823	−25.3120	669.3810	415.3961	2084.4883	3509.2200	1849.0223	–	−49.0748	6.8032	–	–	−100.3419	76–88
$(G - RP)_0$	8027	−5796.4277	–	1747.7036	−308.7685	248.1828	−323.9569	−120.2658	225.9584	–	−35.8856	−16.5715	–	–	48.5619	53–61
$(BP - J)_0$	8172	−2508.6436	442.6771	−24.4624	–	251.5862	−240.7094	86.0579	−11.2705	–	−45.9166	−137.4645	75.3191	−8.7175	21.5739	44–49
$(BP - H)_0$	8159	−2146.1221	368.1630	−23.1719	–	231.8680	−170.8788	52.9164	−6.8455	–	−45.5554	−142.9127	55.2465	−4.1694	17.6593	32–40
$(BP - K_s)_0$	8266	−2124.5574	355.5051	–	–	209.9927	−161.4505	50.5904	−6.3337	–	−27.2653	−160.3595	67.9016	−6.5232	16.5137	24–33
$(RP - J)_0$	9047	−7392.3789	2841.5464	–	−85.7060	–	−88.8397	80.2959	–	−15.3872	54.6816	54.6816	–	−32.9499	−32.9499	91–93
$(RP - H)_0$	8871	−4702.5469	1282.3384	–	−15.8164	–	−30.1373	27.9228	–	−4.8012	25.1870	25.1870	–	−22.3020	−22.3020	52–59
$(RP - K_s)_0$	8911	−4305.9927	1051.8759	–	−8.6045	–	−76.7984	55.5861	–	−3.9681	35.4718	35.4718	–	−16.4448	−16.4448	43–46
$(G - J)_0$	8142	−3003.2988	499.1325	−4.8473	–	244.5030	−303.1783	125.8628	−18.2917	–	−125.8444	59.5183	–	–	16.8172	53–56
$(G - H)_0$	8134	−2573.4998	554.7657	−54.0710	–	229.2455	−206.8658	68.6489	−10.5528	–	−124.5804	41.9630	–	–	7.9258	36–41
$(G - K_s)_0$	8032	−1815.3523	–	70.7201	−1.7309	252.9647	−342.0817	161.3031	−26.7714	–	−120.1133	42.6723	–	–	10.0433	27–31

Note.. Refer to Table 1 for a description of the columns. The same colour limits given in Table 2 apply here. Before using these relations, G, BP, and RP magnitudes for bright sources needs to be corrected for saturation. For sources with two- or six-parameter astrometric solutions G magnitudes must also be corrected (Riello et al. 2021). See Table B1 for extinction coefficients suitable for *Gaia* EDR3 and 2MASS.

APPENDIX B: THE DEPENDENCE OF COLOUR–$T_{\rm EFF}$ RELATIONS ON THE ADOPTED EXTINCTION LAW

The relations of Tables 1 and A1 have been derived adopting the Cardelli et al. (1989)/O'Donnell (1994) extinction law (hereafter COD) for consistency with our earlier work on the IRFM (Casagrande et al. 2010). Here, we investigate the effect of using a different extinction law, namely that of Fitzpatrick (1999), renormalized as per Schlafly & Finkbeiner (2011, hereafter referred to as FSF). Changing law affects the amount of extinction inferred in each photometric band for a given input $E(B - V)$. In other words, different extinction coefficients will be derived. This is due to the fact that extinction laws have different normalizations and shapes. Because of the normalization, extinction coefficients will be higher or lower by a similar per cent. Because of the shape, certain photometric bands will be affected more than others in relative terms. Changes in normalization and shape of extinction laws can also be due to variations in R_V (i.e. the ratio of total to selective extinction in V band, used to build a one-parameter family of curves). In this work, however, we adopt the 'standard' $R_V = 3.1$ which applies to the diffuse interstellar medium for most line of sights in the Galaxy.

Depending on the extinction law, different unreddened colours will be obtained for the same input reddening, thus affecting photometric effective temperatures. The extinction coefficients derived with FSF

are roughly 15 to 25 per cent lower than with COD, implying that $T_{\rm eff}$ of stars affected by reddening will be cooler assuming the former extinction law (Table B1). This is shown in the left-hand panel of Fig. B1, which compares $T_{\rm eff}$ derived using the COD or the FSF law into the IRFM. For the highest reddening values in our sample the difference in temperature can reach up to ~10 per cent, which corresponds to several hundreds of K for hot stars. Fortunately, the effect on the colour–$T_{\rm eff}$ relations is much smaller. For low reddening values (central panel of Fig. B1), bluer or redder stellar colours map into hotter or cooler effective temperature, roughly moving on the same colour–$T_{\rm eff}$ relation, regardless of the underlying extinction law. Thus, even if our relations have been derived using the COD law, a change of extinction coefficients suffices to derive effective temperatures under different extinction curves. This has been verified by using the coefficients in Table B1 with the calibrations of Tables 1 and A1: within the precision allowed by our colour–$T_{\rm eff}$ relations, we are able to recover $T_{\rm eff}$ when the COD or FSD law is implemented in the IRFM directly.

APPENDIX C: SOLAR COLOURS

By fixing the solar surface gravity, metallicity, and effective temperature, equation (1) can be solved to derive the colours of the Sun. Here, we adopt $\log(g)_\odot = 4.44$ and $T_{\rm eff, \odot} = 5777$ K, where the latter

Table B1. Colour-dependent extinction coefficients $R_\zeta = b_0 + b_1(BP - RP)_0 + b_2(BP - RP)_0^2 + b_3(BP - RP)_0^3$ for *Gaia* and 2MASS photometry assuming different laws. To estimate intrinsic colours needed for the fits, one can iterate starting with the assumption $(BP - RP)_0 \simeq (BP - RP) - E(B - V)$.

| | COD extinction law | | | | | | | | FSF extinction law | | | | | | | |
| | Gaia DR2 | | | | Gaia EDR3 | | | | Gaia DR2 | | | | Gaia EDR3 | | | |
	b_0	b_1	b_2	b_3	b_0	b_1	b_2	b_3	b_0	b_1	b_2	b_3	b_0	b_1	b_2	b_3
R_G	3.068	−0.504	0.053	–	3.071	−0.511	0.058	–	2.608	−0.468	0.048	–	2.609	−0.475	0.053	–
R_{BP}	3.533	−0.114	−0.219	0.070	3.526	−0.168	−0.170	0.060	3.007	−0.099	−0.212	0.069	2.998	−0.140	−0.175	0.062
R_{RP}	2.078	−0.073	–	–	2.062	−0.072	–	–	1.702	−0.060	–	–	1.689	−0.059	–	–
R_J	0.899	–	–	–	0.899	–	–	–	0.719	–	–	–	0.719	–	–	–
R_H	0.567	–	–	–	0.567	–	–	–	0.455	–	–	–	0.455	–	–	–
R_{K_s}	0.366	–	–	–	0.366	–	–	–	0.306	–	–	–	0.306	–	–	–

Note.. See discussion in Appendix B for the definition of COD and FSF extinction laws.
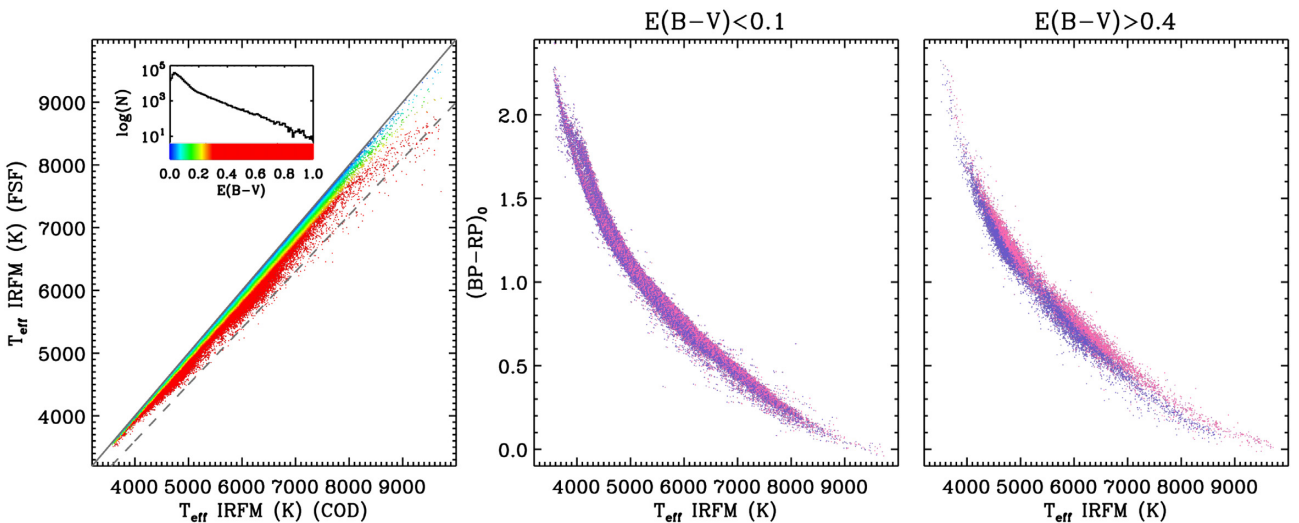

Figure B1. Left-hand panel: comparison between $T_{\rm eff}$ obtained implementing the COD or the FSF extinction law in the IRFM. Stars are colour-coded by their $E(B - V)$ with the distribution shown in the inset. The continuous grey line is the one-to-one relation, whereas the dashed line marks a 10 per cent decrease in $T_{\rm eff}$. Central panel: colour–$T_{\rm eff}$ derived using the COD (pink) and the FSF (purple) extinction laws when reddening is below 0.1. Right-hand panel: same as central panel, but when reddening is above 0.4.
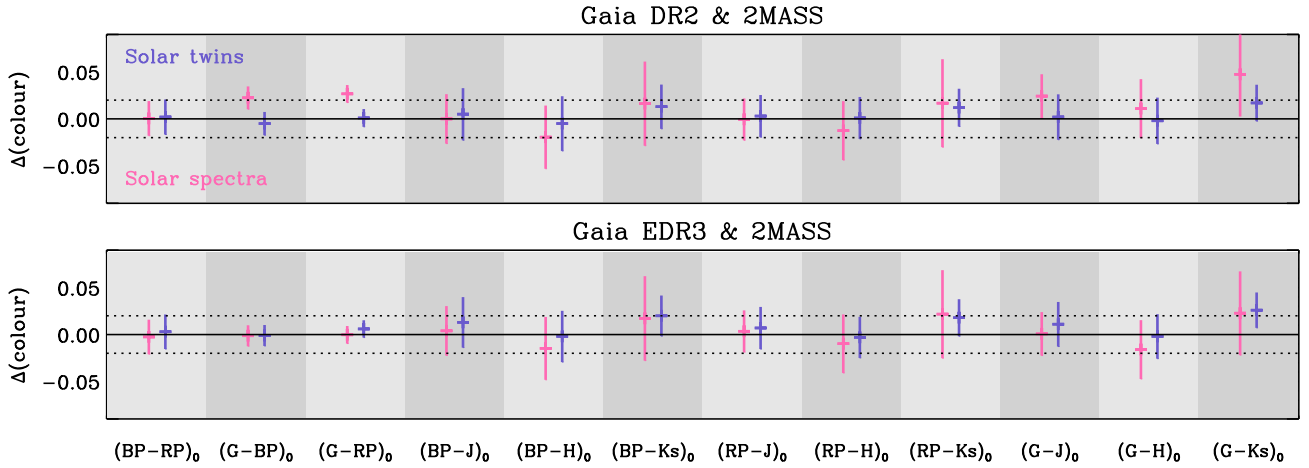
Figure C1. Difference between the colours of the Sun listed in Table C1 and those derived by averaging the colours of four absolutely calibrated solar reference spectra (pink). Error bars are the squared root of the squared sum of the uncertainties reported in Table C1 and of the standard deviation of the colours derived from our four reference spectra. Also shown is the difference between our colours and those inferred from solar twins (blue). Again, error bars are the squared root of the squared sum of the uncertainties in the two data set. The dotted lines mark ± 0.02 mag to give a better sense of the typical agreement across different colour indices.

Table C1. Solar colours.

Colour	Gaia DR2 - 2MASS	Gaia EDR3 - 2MASS
$(BP - RP)_0$	0.823 ± 0.018	0.815 ± 0.018
$(G - BP)_0$	-0.354 ± 0.012	-0.322 ± 0.011
$(G - RP)_0$	0.465 ± 0.009	0.489 ± 0.009
$(BP - J)_0$	1.372 ± 0.025	1.350 ± 0.025
$(BP - H)_0$	1.683 ± 0.025	1.660 ± 0.024
$(BP - K_s)_0$	1.731 ± 0.019	1.712 ± 0.018
$(RP - J)_0$	0.549 ± 0.021	0.538 ± 0.021
$(RP - H)_0$	0.852 ± 0.020	0.843 ± 0.020
$(RP - K_s)_0$	0.907 ± 0.018	0.895 ± 0.018
$(G - J)_0$	1.016 ± 0.022	1.030 ± 0.022
$(G - H)_0$	1.321 ± 0.021	1.338 ± 0.021
$(G - K_s)_0$	1.368 ± 0.016	1.383 ± 0.016

Note.. For the *Gaia* DR2 system, the values provided here supersede those in Casagrande & VandenBerg (2018). The solar absolute magnitude of the averaged flux calibrated spectra is $M_{G,\mathrm{DR2}} = 4.675 \pm 0.006$ and $M_{G,\mathrm{EDR3}} = 4.665 \pm 0.006$.

value is kept for consistency with our previous sets of solar colours (Casagrande et al. 2010, 2012) We verified however that if we were to adopt the effective temperature recommended by the IAU 2015 Resolution B3 (5772 K, Prša et al. 2016) the derived colours would change at most by 0.004 mag, which is considerably less than our uncertainties (where a lower $T_{\mathrm{eff},\odot}$ implies redder solar colours).

In Table C1, we report the colours derived from Tables 1 and A1 for the *Gaia* DR2 and EDR3 system, respectively. The precision $\sigma(T_{\mathrm{eff}})$ quoted for our colour–T_{eff} relations is used to perturb $T_{\mathrm{eff},\odot}$, and to derive uncertainties for the colours of the Sun. The 20 K uncertainty on the zero-point of our effective temperature scale is not included,

and it would typically imply a systematic shift to our colours of order 0.01 mag, depending on the index.

For comparison we also derive solar colours using four high-fidelity, flux-calibrated spectra (from Rieke et al. 2008, the CAL-SPEC solar reference spectrum sun_reference_stis_002, and the solar irradiance spectra of Thuillier et al. 2004 and Meftah et al. 2018). The zero-points and transmission curves used to compute colours from these spectra are the same we have adopted in the IRFM for the *Gaia* DR2, EDR3, and 2MASS system. The agreement between the colours derived from these four spectra is usually very good, the standard deviation being always below 0.008 mag for all indices, except for those involving the H and K_s band (where the standard deviation increases to 0.02–0.04 mag).

Fig. C1 shows that our inferred solar colours are in overall excellent agreement with those obtained from solar reference spectra and solar twins. We use the same solar twins of Table 3, which have an average spectroscopic T_{eff} centred within couple of K from our adopted solar value (depending whether the sample from DR2 – which comprises eight stars – or EDR3 – 10 stars – is used). For the *Gaia* DR2 system, colours map the effective temperature differences already discussed for Table 3. It can be appreciated how well the colours of the Sun from different data set agree, the difference being $\lesssim 0.02$ mag for virtually all bands. In the EDR3 system, the agreement is particularly remarkable for the pure *Gaia* colours $(BP - RP)_0$, $(G - BP)_0$, and $(G - RP)_0$, where our temperature scale, solar twins, and solar spectra all agree to better than 0.006 mag. This is likely indicative of how well EDR3 zero-points and transmission curves are characterized, and how robustly solar colours can now be derived for the *Gaia* system.

This paper has been typeset from a TEX/LATEX file prepared by the author.